Microinterferometric optical phase tomography for measuring small, asymmetric refractive-index differences in the profiles of optical fibers and fiber devices

Brent L. Bachim and Thomas K. Gaylord

A new technique, microinterferometric optical phase tomography, is introduced for use in measuring small, asymmetric refractive-index differences in the profiles of optical fibers and fiber devices. The method combines microscopy-based fringe-field interferometry with parallel projection-based computed tomography to characterize fiber index profiles. The theory relating interference measurements to the projection set required for tomographic reconstruction is given, and discrete numerical simulations are presented for three test index profiles that establish the technique's ability to characterize fiber with small, asymmetric index differences. An experimental measurement configuration and specific interferometry and tomography practices employed in the technique are discussed.

OCIS codes: 060.2270, 110.6960, 180.3170.

1. Introduction

Knowledge of the refractive-index profiles of optical fibers and fiber devices is of critical importance for determining their subsequent performance. For example, the refractive-index profile of dispersion-compensating optical fiber is tailored to achieve specific levels of dispersion at telecommunication wavelengths.[1] Polarization-maintaining optical fiber relies on circular asymmetry present in the fiber structure to decouple orthogonal polarization states. Small, irregular index variations can also affect optical fibers and fiber devices; this is especially true if such variations lead to asymmetry in the transverse refractive-index profile. Birefringence in optical fiber gratings alters transmission spectra and introduces polarization-dependent loss.[2–4] Correct modeling of transmission spectra of fiber gratings that possess arbitrary azimuthal–radial refractive-index variations requires knowledge of the transverse refractive-index profile.[5,6] The form of the index asymmetry must be known if one is trying to reduce birefringence during grating fabrication.[7] To understand and predict the effects of small, asymmetric index variations ($\sim 1 \times 10^{-4}$), it is necessary to measure accurately the refractive-index profiles of optical fiber and fiber devices. It is also desirable to be able to measure index profiles nondestructively to facilitate testing of fiber devices.

Numerous techniques exist for measuring refractive-index profiles of optical fibers and fiber devices. However, many of these techniques require the assumption that the fiber being tested is circularly symmetric. For example, traditional transverse interferometry, although it is nondestructive, assumes circular symmetry when it is profiling optical fibers.[8,9] Similarly, index profiling with the focusing method yields accurate one-dimensional profiles only for circularly symmetric fibers.[10] The implicit assumption of circular symmetry prevents these techniques from being used to characterize irregular, asymmetric index variations in optical fibers.

Additional techniques have been developed for characterizing asymmetry in optical fiber index profiles. Etching combined with atomic-force microscopy provides topographical detail over small regions, but

B. L. Bachim and T. Gaylord (tgaylord@ece.gatech.edu) are with the School of Electrical and Computer Engineering, Georgia Institute of Technology, Atlanta, Georgia 30332-0250. T. K. Gaylord's e-mail address is tgaylord@ece.gatech.edu.

Received 9 February 2004; revised manuscript received 6 October 2004; accepted 8 October 2004.

0003-6935/05/030316-12$15.00/0

quantitative interpretation requires calibration, and the etching process is destructive.[11,12] A variation on the refracted-near-field scanner can measure two-dimensional index profiles but also requires access to an end face and is therefore destructive.[13] Several basic (one-dimensional) profiling techniques have been combined with computed tomography to permit nondestructive measurement of asymmetric index profiles. Profiling of optical fibers in combination with tomography has been demonstrated by use of focusing, multidirectional scattering-pattern, and quantitative phase microscopy approaches. Whereas these combined techniques are effective for profiling typical optical fibers and are nondestructive, they can lack sufficient resolution to detect small, irregular variations in fiber profiles, such as those that could be induced by one-sided exposure to ultraviolet light (typically on the level of 1×10^{-4}). Considering the need to measure accurately small, irregular index variations and the currently available profiling techniques, there is thus a need for a nondestructive measurement technique that permits high-resolution, high-accuracy measurements of small, asymmetric variations in the index profiles of optical fibers and fiber devices.

In this paper we present a measurement technique based on microinterferometry and tomography for use in profiling optical fibers and fiber devices with small, asymmetric index variations over the cross-sectional profile. This technique, microinterferometric optical phase tomography (MIOPT), combines the high-resolution, high-accuracy measurement capabilities of interferometry with the ability to profile irregular objects provided by computed tomography. Using microscopy-based fringe-field interferometry permits detailed inspection of objects such as optical fibers under increased magnification. Characterization of small, asymmetric index changes is important in a number of optical fibers and fiber devices, including elliptical-core polarization-maintaining fiber, twin-core optical fiber, fiber exposed to ultraviolet or carbon dioxide laser light, fiber couplers, and fiber fusion splices.

Interferometry and tomography were combined for index profiling measurements of optical fibers in two previous efforts, neither of which focused primarily on detecting small, asymmetric index variations. The first effort involved characterizing graded-index waveguides that possessed known profile forms (power law) and in which significant ray refraction occurred over sample cross sections.[17] The observed significant ray refraction can be attributed to relatively large refractive-index gradients present in graded-index fibers. The second effort, by Górski, involved profiling optical fibers under conditions of relatively large index differences (greater than 0.015) between fiber cladding and surrounding matching oil.[18] Under such conditions, it becomes difficult to characterize small index changes over an entire cross section, in part because of enhanced diffraction effects. Simulations and measurements made with a bulk interferometer system were conducted for a symmetric multimode optical fiber.

The measurement approach that we present in this paper is concerned with characterizing small index variations ($\sim 1 \times 10^{-4}$) in small objects ($\sim$125-μm diameter). A number of additions and alterations can be made to the combined interferometry and tomography methodology to enhance detection of small index variations. The presence of only small index differences over a cross-sectional profile permits the use of a ray-based, no-deviation formulation that is compatible with established parallel projection computed tomography. Use of commercial interference microscopes to conduct measurements enables control and optimization of interference images to enhance detection of small index differences. Developed interference microscopes also reduce wave-front deviation and diffraction errors and can easily be adapted to perform automated measurements. In the tomography reconstruction process, the acquisition procedure and reconstruction algorithm can be changed to lower noise and enhance detection of small index differences. Through numerical simulations with example optical fiber profiles, we demonstrate that is possible to characterize fibers with small, asymmetric index variations beginning from a set of interference images. The average error in the reconstructed profiles is less than 0.1% for three simulated profiles and results, in part, from implementation of practices to enhance reconstruction accuracy.

We begin the discussion of MIOPT in Section 2 by presenting the ray-based interpretation of the measurement process and include details on what types of measurement must be conducted and on how the information is interpreted and analyzed. Restrictions on using this measurement approach are also discussed. Implementation of interference image analysis and tomographic reconstruction is presented in Section 3. A configuration for collecting the data required for conducting MIOPT by use of an interference microscope is presented in Section 4. Specific ways to improve the detection of small index differences are detailed in Section 5. The results of numerical simulations, used for testing and exploring the analysis portion of the technique, for three different optical fiber profiles are presented in Section 6. Spatial and refractive-index resolution and accuracy issues are addressed in Section 7.

2. Microinterferometric Optical Phase Tomography Theory

Computed tomography permits multidimensional profiling of irregular objects. Such profiling is accomplished through the measurement of a set of projections. For the type of profiling considered here, the projections must be related to the refractive-index values over the optical fiber's transverse cross-section. In this section we discuss the relationship among measured interference images of optical fiber test objects, projections, computed tomography recon-

struction, and the general process for conducting nondestructive characterization. The ray-based approach used for developing the theory is valid for the small index differences considered here and also provides a clear physical understanding of the measurement process.[19]

In the context of measuring two-dimensional transverse refractive-index profiles of optical fibers by use of computed tomography, a set of one-dimensional projection measurements must be collected. An individual projection is a one-dimensional representation of an object that contains both intrinsic property and spatial information.[20] Projections are then used to reconstruct the two-dimensional transverse index profile. Three-dimensional measurements (addition of longitudinal direction) are achieved by stacking two-dimensional reconstructed profiles. In the context of measuring refractive-index profiles, a projection is a line integral of the object's refractive index taken at a specific angle about the object and over its spatial extent. Such a projection can be interpreted as the optical path length over its spatial extent when the object is viewed at a particular angle. The concept of a projection is illustrated in Fig. 1(a) and the notation used in discussing them is shown in Fig. 1(b). The d and L axes represent the rotated coordinate system of the projection and are related to the fixed coordinate system of the object (x and y axes) by projection angle θ. In mathematical terms, a projection, $p(d,\ \theta)$, taken at a particular angle (θ) from the x axis is

$$p(d,\ \theta) = \int_{-\infty}^{\infty} n(d,\ L)\mathrm{d}L, \qquad (1)$$

where $n(d,\ L)$ is the refractive-index profile of the object in the rotated coordinate system. Profile $n(d,\ L)$ is related to $n(x,\ y)$ by a transformation involving angle θ. In practice, the projection integral is taken only over the object's spatial extent.

In developing the theory we consider parallel projections only for use in measuring two-dimensional profiles that possess small index differences. The assumption regarding parallel projections places a restriction on rays traveling through the test object, namely, that no refraction occur. The absence of refraction implies that rays traveling through the sample cross section will always be perpendicular to the d axis in the rotated coordinate system at every projection angle. This restriction cannot be met even in an ideal situation, as some form of index difference always exists in optical fibers (at least at the core–cladding interface) and this causes some rays to be refracted. However, if the refractive index of the surrounding matching oil is closely matched to the sample cladding (within 1×10^{-3}) in an interference microscope system, refraction at the outer boundaries is limited. Other measures can be taken to limit refraction effects and are discussed in Section 5. If proper practices are adopted, the parallel projection approximation for ray travel is valid for use in characterizing fiber samples with small index differences.

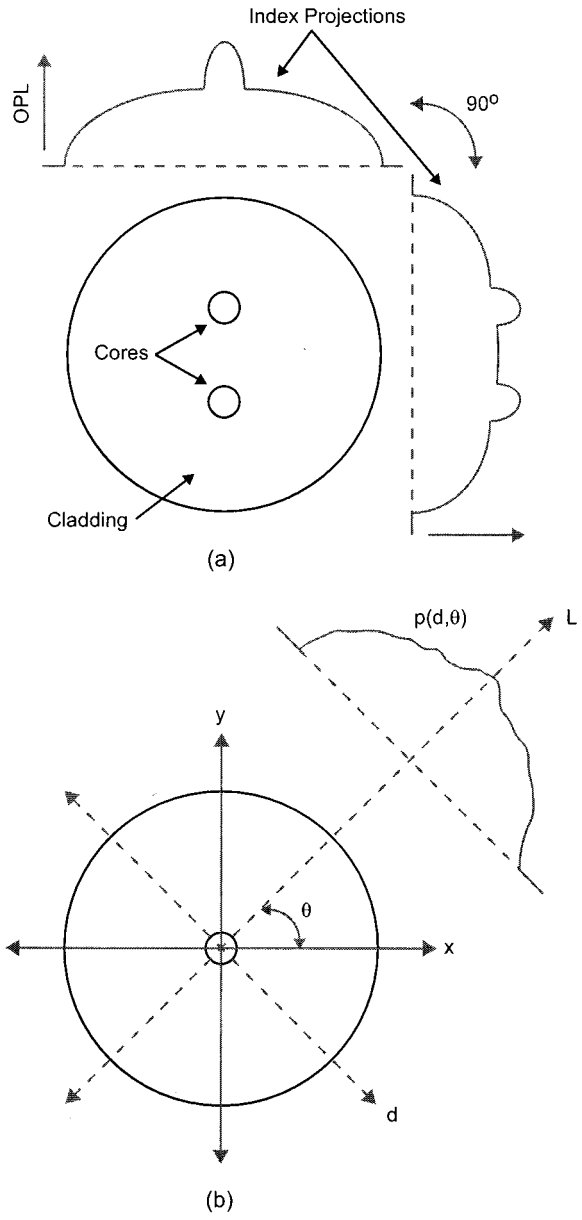

Fig. 1. (a) Illustration of refractive-index projections [optical path length (OPL)] of a twin-core optical fiber taken 90° apart. (b) Relationship between the fixed coordinate system ($x,\ y$) of the optical fiber and the rotated coordinate system ($d,\ L$) of the projection, $p(d,\ \theta)$, at angle θ. The projections go to zero outside the spatial limits of the fiber cross sections.

A set of projections consists of individual projection measurements taken at various angles about the test object. From a set of projections, the object's refractive-index profile can be reconstructed:

$$n(x,\ y) = \int_0^{2\pi} \mathrm{d}\theta \int_0^{\infty} P(\omega,\ \theta)\omega \exp(i2\pi\omega d)\mathrm{d}\omega, \quad (2)$$

where ω is the spatial frequency and $P(\omega, \theta)$ is the Fourier transform of projection $p(d, \theta)$.[20]

One can determine the optical path-length values required for the projection set by measuring phase, as the two are simply related by the free-space wave-vector's magnitude. Several methods exist to measure phase, but one of the most accurate involves interfering an optical wave that has passed through an object with a reference wave. Interference measurement schemes routinely detect optical path differences of less than $\lambda/100$ and thus can detect small changes in index for the same path length. Numerous techniques exist for generating interference images of phase objects,[21–23] but static fringe-field interferometry is considered in the present approach.

Figure 2(a) shows a ray passing through an optical fiber sample. The figure depicts a transverse cross section of a typical single-mode optical fiber but could easily represent another object or device with a more complicated profile. Only one ray is shown in the illustration; a collection of rays at points along the d axis is necessary to produce one projection at each angle θ. The following equations were developed for a ray passing perpendicularly (to the d axis) through the object, as occurs in the rotated projection coordinate system, and are correct for any angle. The mathematical relationship between the measured phase from the interferogram and the projection integral is developed below through examination of the accumulated phase of rays in the sample and reference arms of an interferometer.

The accumulated phase of a ray passing through the optical fiber in the sample arm of the interferometer, δ_{samp}, is given by

$$\delta_{\text{samp}} = k_0 n_{\text{oil}}[L_r - L_f] + k_0 \int_{L_f} n(d, L)\mathrm{d}L, \qquad (3)$$

where k_0 is the free-space wave-vector magnitude, n_{oil} is the refractive index of the matching oil, L_r is an arbitrary reference length, L_f is the length of the sample that the ray traverses (with $L_r > L_f$), and $n(d, L)$ is the two-dimensional refractive-index profile of the optical fiber sample in the rotated coordinate system. The accumulated phase of a matching ray in the reference arm of the interferometer, δ_{ref}, is simply

$$\delta_{\text{ref}} = k_0 n_{\text{oil}} L_r = k_0 n_{\text{oil}}[L_r - L_f] + k_0 n_{\text{oil}} L_f. \qquad (4)$$

As the waves in the two interferometer arms interfere, the phase differences between the sample and the reference result in relative shifts in the minimum–maximum intensity peaks of the static interferogram. The phase difference between rays in the reference and sample beams that pass through the matching oil equals zero and the interference peaks of the rays serve as the baseline for calculating the phase shift that is due to the presence of the sample. The phase difference between reference rays

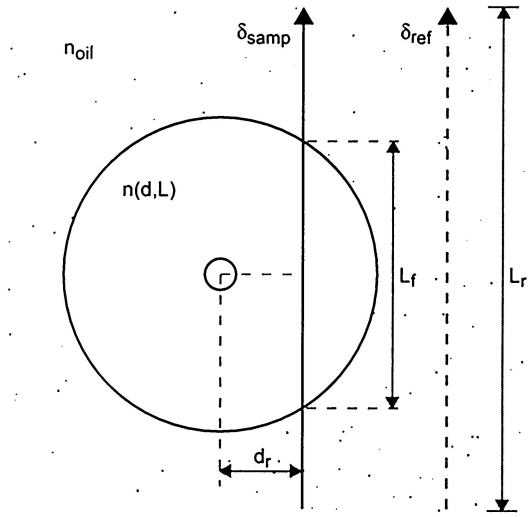

(a)

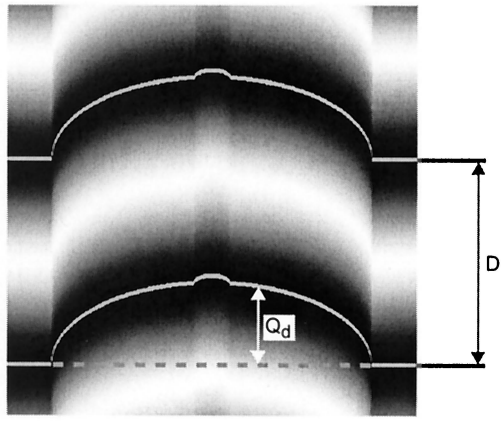

(b)

Fig. 2. (a) Diagram of a typical ray passing through the optical fiber sample. The quantities d and L are the rotated coordinate system axes, $n(d, L)$ is the two-dimensional transverse refractive-index profile of the sample, n_{oil} is the index of the matching oil, δ_{ref} is the phase of a ray traveling through the oil in the reference arm, δ_{samp} is the accumulated phase of a ray traveling through the sample, d_r is the distance from the fiber core to the sample ray, L_f is the length of the sample through which the ray passes, and L_r is an arbitrary reference length. (b) Interference image of optical fiber. D is the fringe separation distance and Q_d is the relative fringe shift.

and rays traveling through the sample are calculated by subtracting Eqs. (3) and (4). This difference is interpreted as the relative phase shift ($\Delta\delta$), with

$$\Delta\delta = \delta_{\text{samp}} - \delta_{\text{ref}} = k_0 n_{\text{oil}}[L_r - L_f] + k_0 \int_{L_f} n(d, L)\mathrm{d}L - k_0 n_{\text{oil}}[L_r - L_f] - k_0 n_{\text{oil}} L_f, \qquad (5)$$

$$\Delta\delta = k_0 \int_{L_f} n(d, L)\mathrm{d}L - k_0 n_{\text{oil}} L_f. \qquad (6)$$

The resultant integral term in Eq. (6) is the projection required for directly implementing computed tomography reconstruction to retrieve the index profile. However, a different form of the integral is more conducive to performing the reconstruction. One can derive the alternative form by rewriting the n_{oil} term in Eq. (6) as

$$k_0 n_{\text{oil}} L_f = k_0 \int_{L_f} n_{\text{oil}} \mathrm{d}L. \tag{7}$$

The integral term in Eq. (7) can then be substituted into Eq. (6) to yield

$$\begin{aligned} \Delta\delta &= k_0 \int_{L_f} n(d,\ L)\mathrm{d}L - k_0 \int_{L_f} n_{\text{oil}} \mathrm{d}L \\ &= k_0 \int_{L_f} [n(d,\ L) - n_{\text{oil}}]\mathrm{d}L. \end{aligned} \tag{8}$$

The integral term containing the difference between $n(d,\ L)$ and n_{oil} can be calculated directly from a recorded interference image and confers the advantage of eliminating the need to calculate L_f during analysis and reconstruction. Although the relative refractive index is now being reconstructed, simply adding the refractive index of the matching oil after the reconstruction is completed yields the desired sample refractive index, $n(x,\ y)$.

Calculating the relative refractive-index projection integral from interference image data requires measuring the relative fringe shift from the baseline fringes that do not pass through the sample and the fringe separation distance. The relative phase shift, $\Delta\delta$, at some distance d_r from the fiber core is calculated from the interferogram by

$$\Delta\delta = \frac{2\pi Q_d}{D} \tag{9}$$

where Q_d is the distance from the baseline fringe reference and D is the separation distance between fringe minima (or maxima) and represents a 2π phase difference.[8] The two values are illustrated in the example interference image shown in Fig. 2(b).

Equating Eqs. (6) and (7) and then rearranging give the relative refractive-index projection integral in terms of the quantities measured from the interference images taken at each projection angle:

$$p_r(d,\ \theta) = \int_{L_f} [n(d,\ L) - n_{\text{oil}}]\mathrm{d}L = \frac{2\pi Q_d}{k_0 D} = \frac{Q_d}{D}\,\lambda_0, \tag{10}$$

where $p_r(d,\ \theta)$ is now the relative index projection. As the physical path is the same, the integral also represents the optical path difference along the d axis. A set of relative projections taken at various angles about the test object can be used to reconstruct the relative-index profile, from which one can determine the actual index profile by adding the matching oil's refractive-index value. Equation (10) has a fundamental relationship to the corresponding equation used for determining the one-dimensional refractive-index profile in traditional transverse interferometry.[8]

From the analysis presented above, it can be seen that MIOPT consists of (1) measuring interference images at a set of projection angles, (2) analyzing the images to extract the phase information, (3) converting the phase information into projection data, (4) collecting the analyzed projection data at all angles, (5) performing computed tomography reconstruction, and (6) adding the matching oil's index to the reconstructed profile to retrieve index profile $n(x,\ y)$.

3. Analysis Implementation

The general measurement procedure described in Section 2 consists of acquiring interference images at many angles about a sample and analyzing the images to perform reconstruction. In this section we discuss specific implementation of the fringe analysis and computed tomography reconstruction portions of the measurements procedure; the experimental configuration for recording interference images is discussed in Section 4.

Implementation of the analysis portion of MIOPT can be separated into two parts: interference fringe analysis and tomographic reconstruction. Splitting the analysis task into two parts allows for flexibility during reconstruction. For instance, the data that result from analyzing interference images can be stored and a variety of reconstruction approaches independently attempted. The particular approaches selected for implementing fringe analysis and computed tomography reconstruction are discussed below. Both the interferogram analysis and the tomographic reconstruction algorithm were implemented discretely (as opposed to the continuous form presented in Section 2).

The static interferogram analysis technique selected for use employs a direct polynomial fitting routine based on parabolic approximation of fringe minima.[21] This approach was used previously in other optical fiber index profiling systems and has the advantage of requiring only one interference image per projection for calculating the phase.[24] A threshold is first applied to the images to locate approximately the fringe minima. Data below the threshold level are retained for use in polynomial fitting. Each pixel column of an interference image is treated as an individual ray for calculation purposes. Therefore the fitting routine is used to identify fringe minima pixel locations along each column. Once the minima locations are known, the relative-index projection can be calculated [from the right-hand side of Eq. (10)]. All images captured during measurement are analyzed

to extract their phase, which is used to calculate the projection.

The second portion of the analysis procedure, tomographic reconstruction, was implemented by use of the filtered backprojection algorithm.[20] Again, a number of reconstruction algorithms exist, but the filtered backprojection algorithm is a well-established technique in tomography that provides flexibility for optimizing the reconstruction process to increase accuracy. The projections derived from interference images taken at various angles serve as the input to the algorithm. Basically, the algorithm involves taking the Fourier transform of each projection, applying a reconstruction filter to it, and then performing an inverse Fourier transform. The filtered projection is then backprojected to form a square matrix; the matrix is rotated by the corresponding projection angle (θ) and then added to previously processed backprojection matrices. Object reconstruction is complete when all projections have been processed and the matching oil's index value is added.

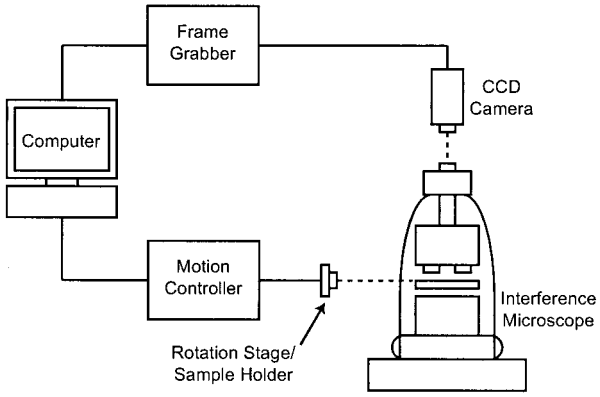

Fig. 3. Experimental configuration for measuring interference images of an optical fiber test object at various projection angles. An optical fiber sample, secured in the holder, can be rotated about its axis to enable interference images to be recorded at any angle. The measurement system is automated easily by incorporation of a motion controller and a frame grabber.

4. Experimental Configuration

A microinterferometer arrangement, with associated hardware, is necessary for obtaining interference images of optical fiber and fiber devices to perform profiling. Although it is possible to construct an apparatus for conducting measurements from bulk optical elements, several interference microscopes already exist that are suitable for use in the system.[8,25,26] Using a commercial interference microscope confers many advantages, which we addressed in Section 5 below. An interference microscope suitable for conducting MIOPT measurements is described below, along with the overall experimental configuration.

The Mach–Zehnder two-objective, transmitted-light interference microscope that is traditionally used for profiling symmetric optical fibers can be adapted to facilitate interference measurements at various angles.[8,25] Adapting the microscope requires only the addition of a rotary stage, a sample holder–positioner, and a motion controller to the traditional arrangement, as the system already includes a camera and a frame grabber for capturing interference images. A diagram of the overall experimental configuration is shown in Fig. 3. The measurement process, in this arrangement, can be automated to reduce the amount of time required for taking the large number of projections needed for low-noise reconstruction. The microscope (originally manufactured by Ernst Leitz GmbH, Wetzlar, Germany), is found in many optical fiber characterization laboratories because it is currently used for profiling circularly symmetric optical fiber.

5. Measurement Optimization for Characterizing Small, Asymmetric Index Differences

Characterizing small asymmetric index differences in the refractive-index profiles of optical fibers and fiber devices requires consideration of the measurement procedures associated with fringe-field interferometry and tomography. Additions and alterations to the basic interferometry and tomography approaches can lower noise levels and enhance detection of small index differences. Methods for improving detection are identified and discussed in this section.

Use of a developed commercial interference microscope, as opposed to implementation of a bulk optic interferometer,[18] offers several advantages for conducting this type of measurement. Interference microscopes, such as the Mach–Zehnder transmitted-light system discussed in Section 4, are designed to have precise, stable optical elements that minimize wave-front distortion and maintain path balance and thereby increase interference-image stability. Optical plates and wedges incorporated within the microscope permit precise adjustment of fringe spacing, orientation, and width. The ability to conduct precise adjustments means that fringe properties can be optimized for detecting small index differences. Spurious fringes and speckle noise are reduced by use of a bright, bandpass-filtered mercury lamp instead of a laser-based illumination system commonly employed in bulk systems. With the automated measurement configuration shown in Fig. 3, multiple images can be captured at each projection angle and averaged to reduce noise effects.

Using an interference microscope to conduct measurements has the additional advantage of reducing refraction effects. As mentioned above, optical fiber samples must be surrounded with an accurately known index-matching oil whose refractive-index value is close to (but not equal to) that of the sample outer cladding. Matching the indices of the oil and cladding lowers the deviation of the rays at the surface boundaries.[27] Direct use of high-magnification oil-immersion objectives ensures that the matching criteria will be met and eliminates the need for microscope slides and coverslips that can introduce wave-front distortion. In situations when the index

value of the cladding is not known, oils with different refractive indices can be tried until a suitable fringe field is observed. In addition to facilitating precise matching, the microscopy approach presented corrects for some refraction effects when the system is properly focused on the center of the fiber.[27] Even with the two corrective measures suggested, samples such as graded-index and air–silica microstructure optical fibers would not meet the parallel projection criteria owing to excessive ray refraction over their transverse cross sections. However, as our concern is primarily with measuring small perturbations in index profiles of commercial telecommunications fiber, refraction effects owing to asymmetry are expected to be below those that are due to interfaces (oil–cladding and core–cladding). In cases of excessive refraction, a different form from parallel projections may be adopted in describing ray paths through the sample (for example, a fan-beam projection[20]). Ray tracing offers one method for investigating whether a particular optical fiber sample would introduce too much deviation.[18,27]

Consistent with the primary purpose of detecting small variations in refractive index, several portions of the measurement and analysis procedures can be changed within the reconstruction process to lower noise levels and subsequently improve detection of small variations in refractive index. Taking projections over a full 360°, taking additional projections, and employing various reconstruction filters all act to lower noise levels in certain regions of reconstructed objects. Taking projections 360° around the sample object, instead of over just 180°, increases averaging of noisy data and reduces asymmetric ringing effects.[28] Increasing the total number of projections (decreasing the angle between projections) also leads to increased averaging of noisy data.[28] Altering the reconstruction filter (part of the filtered backprojection algorithm) to introduce averaging and attenuation of higher frequencies lowers the noise level and improves the changes of detecting small variations within interior regions but not near edges or sharp transitions.[19,20,28] Various effects of the type of filter used in reconstruction are demonstrated in Section 6 below.

By incorporating all the additions and alterations discussed in this section into the MIOPT measurement process, the ability to detect small, asymmetric index changes is improved. The effect of some of these changes can be illustrated through numerical simulations.

6. Simulations and Simulation Results

To evaluate the proposed measurement methodology, to test the analysis programs, and to verify the ability to profile asymmetric objects we conducted a series of discrete numerical simulations. Three optical fiber transverse cross sections were generated, from which interference images were created. The generated interference images served as simulated inputs to the fringe analysis and reconstruction programs. The specific details of interferogram analysis and tomographic reconstruction implementation are given below, along with results for the three different types of simulated profile. The method for generating the interference images by use of the MATLAB programming language is also given. The average error in the reconstructed refractive-index profiles was less than 0.1%, depending on the type of reconstruction filter employed and on whether there is any postreconstruction image processing. Using the simulations, we demonstrate that it is possible to reconstruct accurately refractive-index profiles with small, asymmetric index differences from a set of measured interference images taken at various angles about the test object.

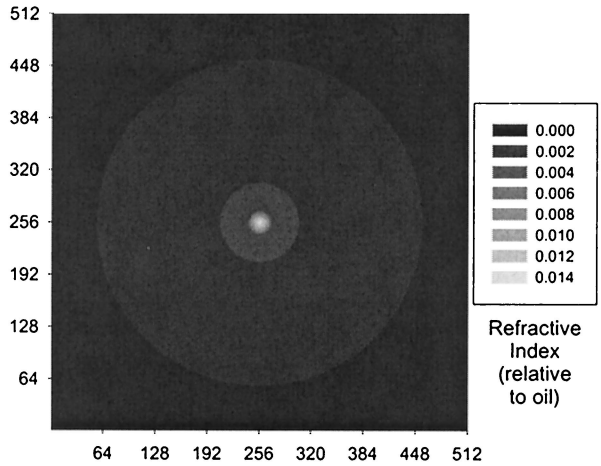

Fig. 4. Gray-scale plot of a transverse optical fiber refractive-index profile relative to the matching oil's index. Simulated profiles like this one are used for generating interference images and testing the fringe analysis reconstruction programs. This particular simulated profile is circularly symmetric and possesses outer cladding, inner cladding, and core regions.

To begin the simulation, a desired cross-sectional refractive-index profile of an optical fiber is generated as a 512×512 matrix, with the fiber surrounded by an index-matching oil. The optical fiber index profile matrix is subtracted from another constant-valued (n_{oil}) matrix of the same dimensions, and the result is multiplied by the image pixel spacing (ΔL). The resultant matrix serves as the basis for calculating the phase used in generating the interference image for each projection angle. An example relative refractive-index profile is shown in Fig. 4. The difference matrix is then rotated by the current projection angle and its columns summed to generate an array containing the optical path difference that is due to the object. For all three simulations, projections were taken every 0.5° about the generated profile (720 projections total for each simulation). The large number of projections reduces noise levels in the reconstructed image.

The interference images used for evaluating the tomographic process were generated from Kingslake's formulation, which is given by

$$I(p, q) = \{A + B \cos[k_0 W(p, q)]\} + N(p, q), \quad (11)$$

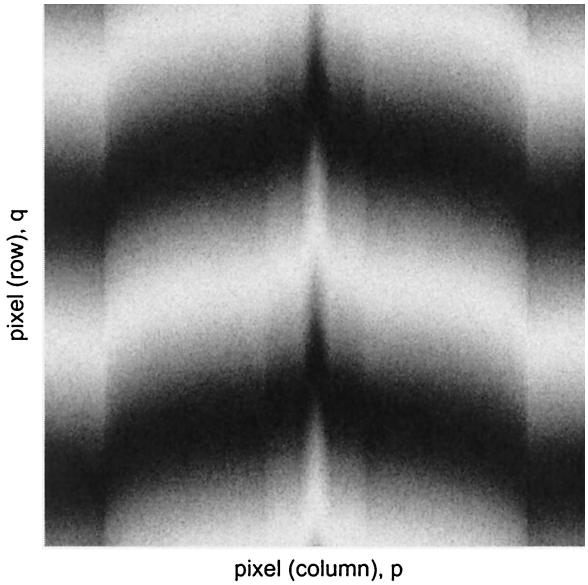

Fig. 5. Example interference image generated by use of Eq. (11) from the test profile shown in Fig. 3. As the profile is symmetric, all the projections are identical (except for additive noise).

where p and q are, respectively, the columns and rows of the image, $I(p, q)$ is the irradiance in the interferogram plane, A is the static bias, B is the amplitude, $W(p, q)$ is the optical path difference, and $N(p, q)$ is the noise added to the interference image.[29] The irradiance, static bias, and amplitude are given in terms of an 8-bit gray scale (0–255), as would be captured from a typical CCD camera. We calculated the optical path difference by first generating a matrix with the dimensions of the image and that possesses a linear optical path variation along its columns but an optical path that is constant across its rows. This configuration mimics the interference of two waves that are tilted with respect to each other to create carrier fringes. Another matrix, with the same dimensions as the carrier fringe matrix, is created with the projection optical path-difference array (representing the phase effect of the sample) and is added to the carrier fringe matrix. After the complete interference image is calculated, Gaussian noise is added that possesses a zero mean and standard deviation σ_m.[29,30] A noisy interference image is generated for each projection taken of the test index profile and saved in an image file format similar to that of experimentally acquired images. The entire image set for a particular test profile served as the input to the fringe analysis program. A typical interference image generated from the index profile in Fig. 4 is shown in Fig. 5. The values of parameters used in generating the interference images for all three simulated cross sections are as follows: A, 128; B, 108; λ_0, 546 nm; μ, 0; σ_m, 8; and ΔL, 312.5 nm. The mean noise (μ) and standard deviation (σ_m), similar to the static bias (A) and amplitude (B), are in terms of gray-scale digital numbers that represent intensity levels.

In generating the interference images we followed the parallel projection (no refraction) assumption.

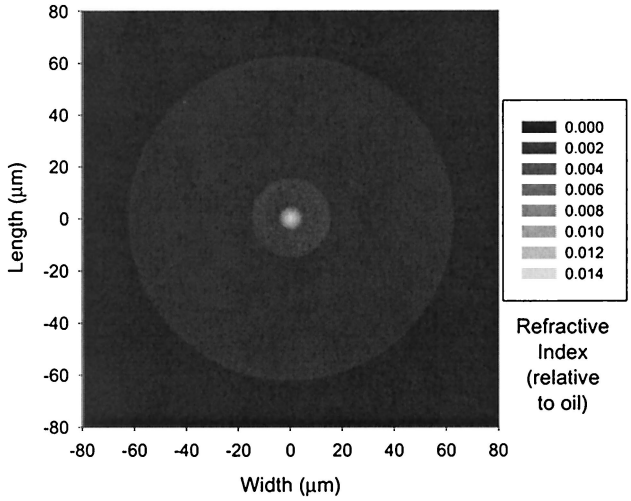

Fig. 6. Gray-scale plot of the reconstructed index profile of the circularly symmetric optical fiber.

Therefore any variations in the gray-scale intensity are due only to changes in phase. It was also assumed that sample rotation occurred exactly axially, implying that tilt and shifting of the sample cross-section center location (center of fiber core) are not factors. In practice, tilting and shifting of sample objects in images can be compensated for if they are found to occur.[31]

The first simulated profile was that of a circularly symmetric optical fiber with an inner cladding, an outer cladding, and a core, the same as that shown in Fig. 4. A symmetric profile was simulated initially to test the programs, as it represents a simple, known profile. The reconstructed object profile, after the simulated interference images have been processed by use of the interferogram analysis and reconstruction programs, is shown in Fig. 6. The maximum error in the reconstructed profile over the entire cross section was 0.12%, and the average, 0.002%. Specific results are shown in Fig. 7(a) for a line section of the profile along its length at the center width. Figure 7(b) shows the absolute difference between the test and the reconstructed profiles. The reconstructed profile matches the generated test profile closely. All profiles from Fig. 4 to Fig. 11 have been plotted relative to the matching-oil index to enhance illustration of index variations. Only the refractive-index value of the matching oil (1.4571) must be added to yield the absolute index profiles. A modified reconstruction filter (typical ramp-type combined with a Hanning filter) was used to enhance the accuracy in interior regions of the profile, with a corresponding decrease in accuracy near edges and sharp transitions.[20,28]

Next, a twin-core optical fiber was simulated with a profile similar to that in the research of Barty *et al.* (measured by quantitative phase microscopy).[16] This fiber is not circularly symmetric, as can be seen from Fig. 8(a), and is therefore useful for evaluating the ability of the present method to characterize asymmetric objects. The reconstructed object profile is shown in Fig. 8(b). The maximum error in the recon-

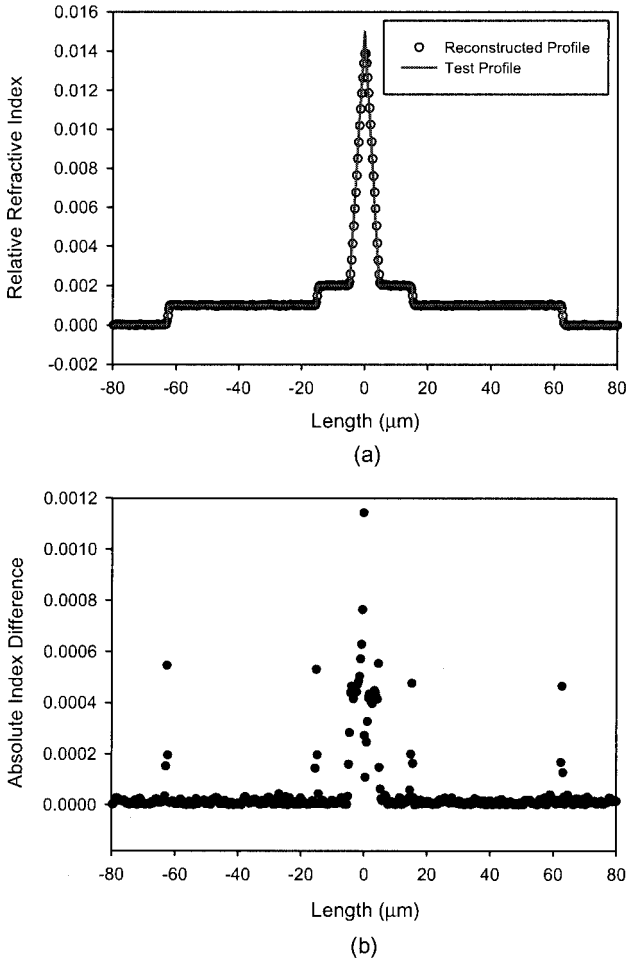

Fig. 7. Symmetric optical fiber simulation results. (a) Comparison of test and reconstructed profiles taken along the length at the center of the width. (b) Absolute index difference between test and reconstructed profiles shown in (a). The noise in the interior cladding regions is lower than that near the edges and in the core because of the modified filter used in reconstruction.

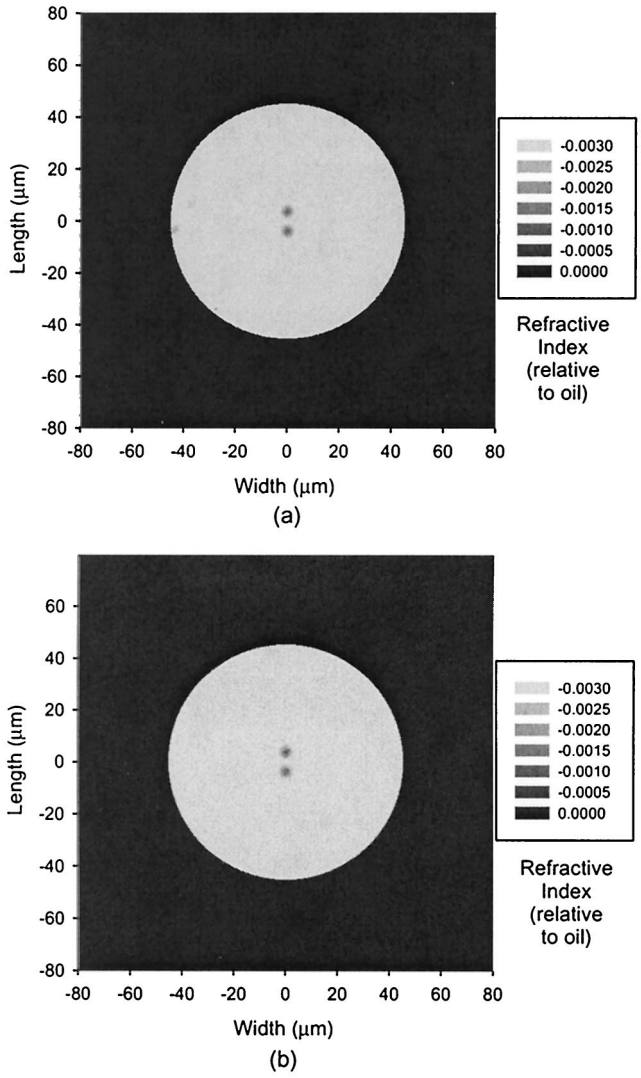

Fig. 8. (a) Gray-scale plot of the generated transverse refractive-index profile of a twin-core optical fiber relative to the matching oil's index. The profile is not circularly symmetric because of the two offset (from center) cores. (b) Reconstructed index profile.

structed profile over the entire cross section was 0.21%; and the average, 0.083%. Specific results, following processing, are shown in Fig. 9(a) for a line section of the profile along its length at the center width. Figure 9(b) shows the absolute difference between the test and reconstructed profiles. The error is larger over the entire profile for this reconstruction, in contrast to the profile shown in Fig. 7(b), because only the required ramp-type filter (unmodified) was used for the reconstruction. The error is larger, though more nearly uniform, over the line section, and the core features are better preserved.

The third profile, a single-mode optical fiber with an exponential variation over the cross section, is shown in Fig. 10(a). The index profile is circularly asymmetric and has one side of the cladding at a slightly higher index value than the other side (1.5×10^{-4}), with exponential variation between. The asymmetry in the profile is similar to that observed in optical fibers exposed to ultraviolet light but applied over the entire cross section and not simply in the core. Optical fibers exposed to carbon dioxide laser light have approximately this form of small index asymmetry. The reconstructed object profile is shown in Fig. 10(b). The maximum error in the reconstructed profile over the entire cross section was 0.08%; and the average, 0.002%. Specific results, following processing, are shown in Fig. 11(a) for a line section of the profile along its length at the center width. Figure 11(b) shows the absolute difference between the test and reconstructed profiles. Because the exponential variation is concentrated predominantly within the cladding, a modified reconstruction filter (the same as was used for the symmetric profile simulation) was used to achieve lower error in the cladding regions.

The results of the simulations demonstrate that it is indeed possible to reconstruct the index profiles of optical fibers with index asymmetry and small index differences by analyzing interference images taken at

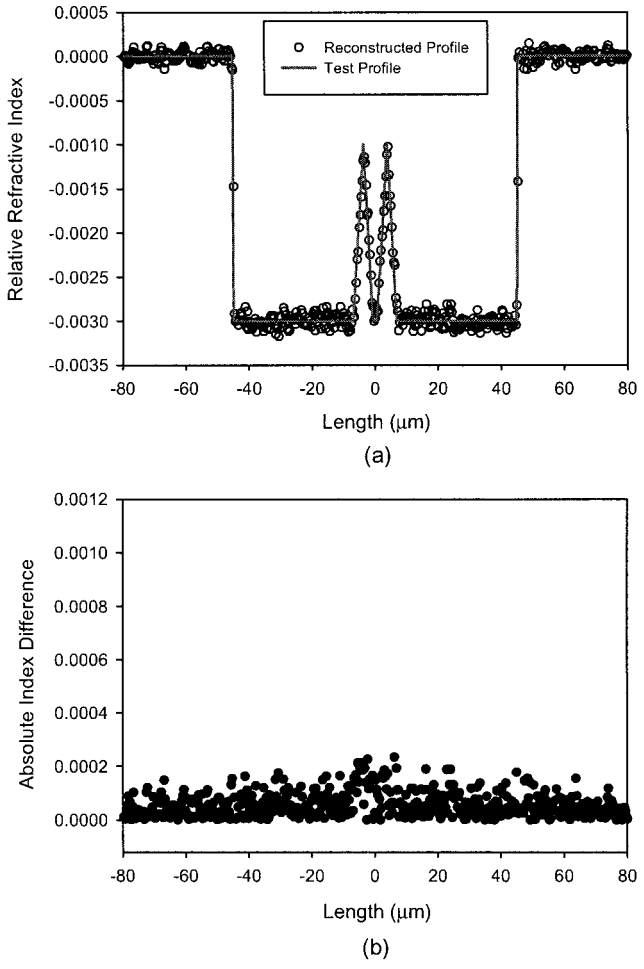

Fig. 9. Twin-core optical fiber simulation results. (a) Comparison of test and reconstructed profiles taken along the length at the center of the width. (b) Absolute index difference between test and reconstructed profiles shown in (a). Noise levels are roughly similar in the cladding and cores and near the edges because only the basic ramp-type filter was used.

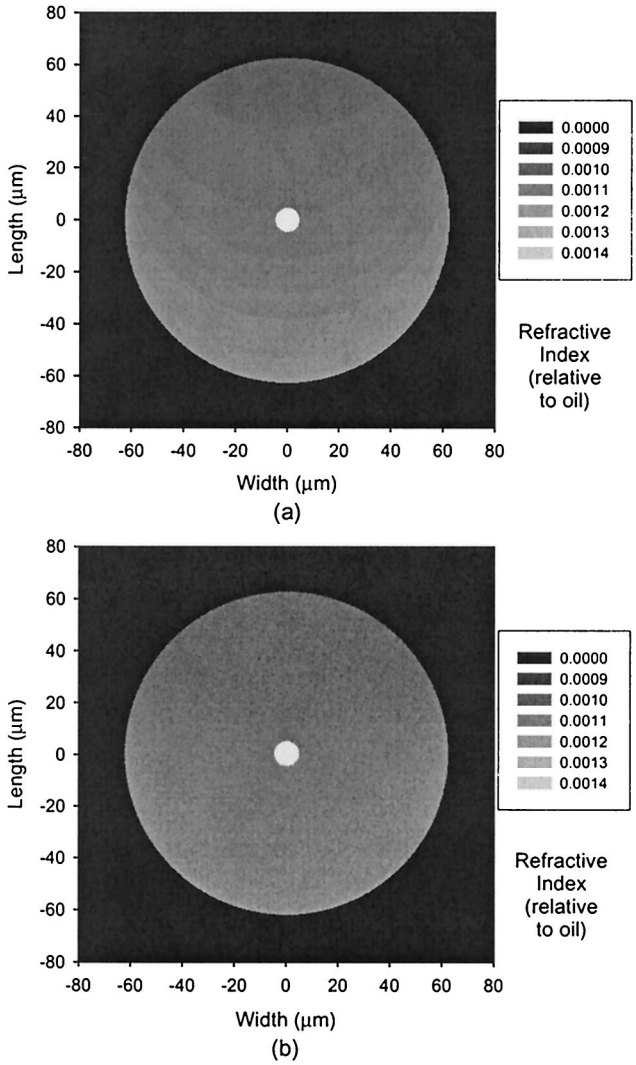

Fig. 10. (a) Gray-scale plot of the generated transverse refractive-index profile of a single-mode optical fiber relative to the matching oil's index. The exponential variation originates from one side and was calculated from an equation of Dossou *et al.*[5], but applied over the entire cross section. (b) Reconstructed index profile. A shorter relative index range is used to highlight index variations in the cladding region (core features are not shown).

multiple angles and using computed tomography. They also show how one can change reconstruction to emphasize certain aspects (such as interior regions) by modifying the basic ramp-type reconstruction filter used in the filtered backprojection algorithm to attenuate selected spatial frequencies. Modifying the filter can be useful when one is attempting to profile fibers with small index variations in, for instance, the cladding region.

7. Resolution and Accuracy

High resolution and high accuracy, in both spatial and refractive-index terms, are two of the advantages offered by using microinterferometry to conduct profiling. The factors that influence resolution and accuracy are different for the refractive-index and spatial domains; the issues are far more complicated for the index case.

Spatial resolution is determined by distinct factors in the transverse (cross-sectional) and axial directions. The transverse spatial resolution is set by a combination of the microscope's lateral resolving power and the equivalent pixel spacing of the CCD camera at a given magnification. For the Mach–Zehnder transmitted light microscope discussed in Section 4 the lateral resolvable power is approximately 0.5 μm at 50× magnification.[32] For example, if the equivalent pixel spacing of a typical CCD camera at that magnification is approximately 0.6 μm, then the pixel spacing limits the transverse spatial resolution because it is the larger value. Axial spatial resolution is set by the fringe separation distance. In calculating the relative phase shift from interference images, the phase difference between fringe minima is assumed to be the same. The assumption is necessary for scaling relative shifts to a known phase value (2π). For the assumption to be true, the transverse

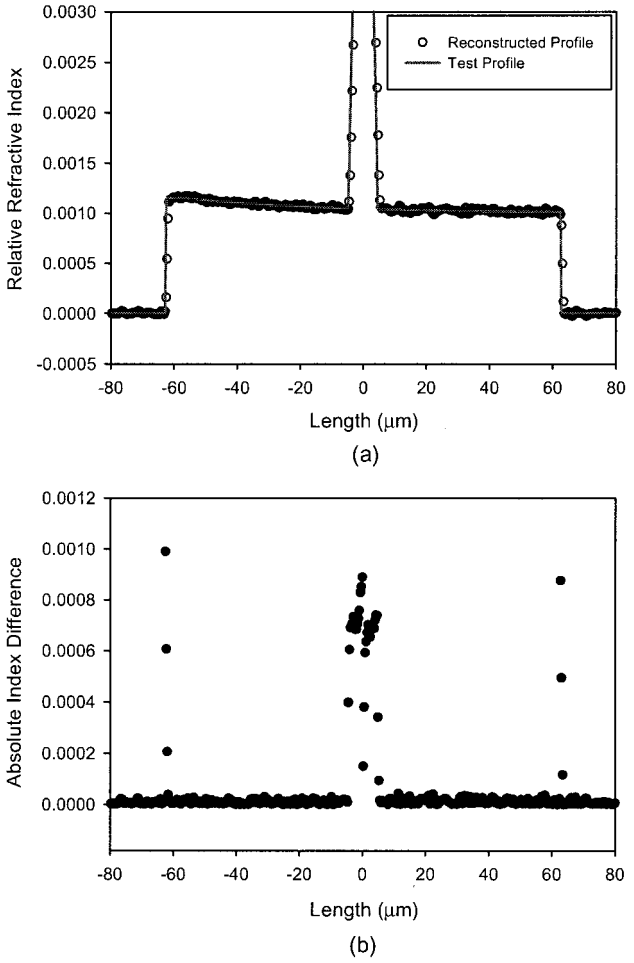

Fig. 11. Asymmetric (exponential) profile optical fiber simulation results. (a) Comparison of test and reconstructed profiles taken along the length at the center of the width. The exponential variation over the length is evident in the reconstructed profile. (b) Absolute index difference between test and reconstructed profiles shown in (a).

index profile must be constant along the axial direction. In the example interferogram shown in Fig. 5, the fringe separation distance is approximately 100 μm, and that value represents the axial spatial resolution limit. The fringe separation can be decreased to improve axial resolution but only with an accompanying reduction in the ability to detect small changes in phase. The spatial resolution gained by using microinterferometry permits profiling of samples with more rapidly varying radial changes, as occurs in dispersion-compensating fiber, than in typical optical fiber.

Refractive-index resolution and accuracy are more complicated than their spatial equivalents. Noise levels in the reconstructed image depend not only on the smallest detectable fringe shift difference but also on tomography reconstruction practices. The smallest detectable fringe shift difference is influenced by environmental factors, system noise, and the fringe analysis program. Factors that influence index resolution originating from computed tomography include the type of algorithm used for reconstruction, filters, the number of projections taken, and the number of samples per projection.[28] In addition, the accuracy of the reconstructed object can vary in different regions (interior versus edge). No models exist for predicting the signal-to-noise ratio for a measurement approach such as MIOPT, though simplified noise models are available for traditional (x-ray) computed tomography.[28,33] Quantitative signal-to-noise ratio values are usually established through measurements of a uniform phantom.[20] Despite the complexity inherent in the process, the simulation results give a general idea of the noise that arises from the analysis portion of the measurement process.

8. Summary

Microinterferometric optical phase tomography combines the ability to detect small refractive-index changes found in fringe-field interferometry with the ability to characterize irregular objects offered by computed tomography. In this paper we have presented and discussed the underlying theory of MIOPT, analysis implementation, numerical simulation results, experimental configurations, and resolution and accuracy issues. MIOPT is unique among the various profiling techniques in that it was intentionally designed to characterize small, asymmetric index perturbations in optical fibers and fiber devices.

The research of B. L. Bachim was sponsored in part by a National Science Foundation graduate research fellowship.

References

1. L. Grüner-Nielsen, S. N. Knudsen, B. Edvold, T. Veng, D. Magnussen, C. C. Larsen, and H. Damsgaard, "Dispersion compensating fibers," Opt. Fiber Technol. **6,** 164–180 (2000).
2. T. Erdogan and V. Mizrahi, "Characterization of UV-induced birefringence in photosensitive Ge-doped silica optical fibers," J. Opt. Soc. Am. B **11,** 2100–2105 (1994).
3. Y. Ishii, K. Shima, S. Okude, K. Nishide, and A. Wada, "PDL suppression on long-period fiber gratings by azimuthally isotropic exposure," IEICE Trans. Electron. **E85-C,** 934–939 (2002).
4. B. L. Bachim and T. K. Gaylord, "Polarization-dependent loss and birefringence in long-period fiber gratings," Appl. Opt. **42,** 6816–6823 (2003).
5. K. Dossou, S. LaRochelle, and M. Fontaine, "Numerical analysis of the contribution of the transverse asymmetry in the photo-induced index change profile to the birefringence of optical fiber," J. Lightwave Technol. **20,** 1463–1470 (2002).
6. E. Anemogiannis, E. N. Glytsis, and T. K. Gaylord, "Transmission characteristics of long-period fiber gratings having arbitrary azimuthal/radial refractive index variations," J. Lightwave Technol. **21,** 218–227 (2003).
7. A. M. Vengsarkar, Q. Zhong, D. Inniss, W. A. Reed, P. J. Lemaire, and S. G. Kosinski, "Birefringence reduction in side-written photoinduced fiber devices by a dual-exposure method," Opt. Lett. **19,** 1260–1262 (1994).
8. L. M. Boggs, H. M. Presby, and D. Marcuse, "Rapid automatic index profiling of whole-fiber samples. 1," Bell Syst. Tech. J. **58,** 867–882 (1979).

9. D. Marcuse and H. M. Presby, "Focusing method for nondestructive measurement of optical fiber index profiles," Appl. Opt. **18,** 14–22 (1979).
10. Y. Kokubun and K. Iga, "Precise measurement of the refractive index profile of optical fibers by a nondestructive interference method," Trans. IECE Japan **E60,** 702–707 (1977).
11. Q. Zhong and D. Inniss, "Characterization of the lightguiding structure of optical fibers by atomic force microscopy," J. Lightwave Technol. **12,** 1517–1523 (1994).
12. S. T. Huntington, P. Mulvaney, A. Roberts, K. A. Nugent, and M. Bazylenko, "Atomic force microscopy for the determination of refractive index profiles of optical fibers and waveguides: a quantitative study," J. Appl. Phys. **82,** 2730–2734 (1997).
13. N. H. Fontaine and M. Young, "Two-dimensional index profiling of fibers and waveguides," Appl. Opt. **38,** 6836–6844 (1999).
14. K. Toga, N. Amano, and K.-I. Noda, "Microscopic computer tomography measurement of nonaxisymmetrically distributed optical fiber refractive index," J. Lightwave Technol. **6,** 73–79 (1988).
15. T. Okoshi and M. Nishimura, "Measurement of axially nonsymmetrical refractive-index distribution of a single-mode fiber by a multidirectional scattering-pattern method," J. Lightwave Technol. **1,** 9–14 (1983).
16. A. Barty, K. A. Nugent, A. Roberts, and D. Paganin, "Quantitative phase tomography," Opt. Commun. **175,** 329–336 (2000).
17. N. Barakat, H. A. El-Hennawi, E. A. El-Ghafar, H. El-Ghandoor, R. Hassan, and F. El-Diasty, "Three-dimensional refractive index profile of a GRIN optical waveguide using multiple beam interference fringes," Opt. Commun. **191,** 39–47 (2001).
18. W. Górski, "The influence of diffraction in microinterferometry and microtomography of optical fibers," Opt. Lasers Eng. **41,** 563–583 (2004).
19. W. Górski and M. Kujawińska, "Three-dimensional reconstruction of refractive index inhomogeneities in optical phase elements," Opt. Lasers Eng. **38,** 373–385 (2002).
20. J. Hsieh, *Computed Tomography: Principles, Design, Artifacts, and Recent Advances* (SPIE Press, Bellingham, Wash., 2003).
21. J. Schwider, "Advanced evaluation techniques in interferometry," in *Progress in Optics*, E. Wolf, ed. (Elsevier, New York, 1990), Vol. 28, pp. 271–359.
22. M. Sochacka, "Optical fiber profiling by phase-stepping transverse interferometry," J. Lightwave Technol. **12,** 19–23 (1994).
23. B. V. Dorrio and J. L. Fernández, "Phase-evaluation methods in whole-field optical measurement techniques," Meas. Sci. Technol. **10,** R33–R55 (1999).
24. D. Marcuse and H. Presby, "Index profile measurements of fibres and their evaluation," Proc. IEEE **68,** 666–688 (1980).
25. M. Pluta, *Measuring Techniques, Vol. 3, Advanced Light Microscopy* (Elsevier, New York, 1993).
26. M. Pluta, "Profile refractometry of optical fibers using double-refracting microinterferometry," in *Gradient-Index Optics in Science and Engineering*, M. Pluta and M. Szyjer, eds., Proc. SPIE **2943,** 113–127 (1996).
27. Y. Park, S. Choi, U. C. Paek, K. Oh, and D. Y. Kim, "Measurement method for profiling the residual stress of an optical fiber: detailed analysis of off-focusing and beam-deflection effects," Appl. Opt. **42,** 1182–1190 (2003).
28. D. A. Viskoe and G. W. Donohoe, "Optimal computed tomography data acquisition techniques and filter selection for detection of small density variations," IEEE Trans. Instrum. Meas. **45,** 70–76 (1996).
29. S. Vázquez-Montiel, J. J. Sánchez-Escobar, and O. Fuentes, "Obtaining the phase of an interferogram by use of an evolution strategy. 1," Appl. Opt. **41,** 3448–3452 (2002).
30. J. M. Gauch, "Noise removal and contrast enhancement," in *The Colour Image Processing Handbook*, S. J. Sangwine and R. E. N. Home, eds. (Chapman & Hall, New York, 1998), pp. 149–162.
31. A. Barty, "Quantitative phase-amplitude microscopy," Ph.D. dissertation (University of Melbourne, Parkville, Victoria, Australia, 2000).
32. Ernst Leitz GmbH, "Transmitted-light interference microscope instructions," (Ernst Leitz, Wetzlar, Germany, 1971).
33. H. H. Barrett and W. Swindell, *Radiological Imaging: The Theory of Image Formation, Detection, and Processing* (Academic, New York, 1981), Vol. 2.